This is a repository copy of *Measuring grain boundary segregation: tomographic atom probe field ion microscopy (APFIM) vs. analytical scanning transmission electron microscopy (STEM)*.

White Rose Research Online URL for this paper:
http://eprints.whiterose.ac.uk/146747/

Version: Published Version

Proceedings Paper:

Walther, T. orcid.org/0000-0003-3571-6263 (2019) Measuring grain boundary segregation: tomographic atom probe field ion microscopy (APFIM) vs. analytical scanning transmission electron microscopy (STEM). In: Journal of Physics: Conference Series. 19th International Conference on Extended Defects in Semiconductors (EDS2018), 24-29 Jun 2018, Thessaloniki, Greece. IOP Publishing .

https://doi.org/10.1088/1742-6596/1190/1/012002

Reuse
This article is distributed under the terms of the Creative Commons Attribution (CC BY) licence. This licence allows you to distribute, remix, tweak, and build upon the work, even commercially, as long as you credit the authors for the original work. More information and the full terms of the licence here: https://creativecommons.org/licenses/

Takedown
If you consider content in White Rose Research Online to be in breach of UK law, please notify us by emailing eprints@whiterose.ac.uk including the URL of the record and the reason for the withdrawal request.

eprints@whiterose.ac.uk
https://eprints.whiterose.ac.uk/

IOP Conf. Series: Journal of Physics: Conf. Series **1190** (2019) 012002 doi:10.1088/1742-6596/1190/1/012002

Measuring grain boundary segregation: tomographic atom probe field ion microscopy (APFIM) vs. analytical scanning transmission electron microscopy (STEM)

T Walther

Department of Electronic & Electrical Engineering, University of Sheffield, George Porter Building, North Campus, Wheeldon Street, Sheffield S3 7HQ, UK

t.walther@sheffield.ac.uk

Abstract. Grain boundary segregation is an important phenomenon in metallurgy and semiconductor technology. Some recent studies by tomographic atom probe field ion microscopy (APFIM) claim to have measured the interfacial excess of atoms segregated to grain boundaries with ultra-high precision, down to 0.01-0.02 atoms/nm^2. This study critically evaluates these claims by simulations. It is shown that atom probe tomography is no 'magic bullet' and suffers similar physical constraints as analytical scanning transmission electron microscopy (STEM). Data analyses from both methods have much in common in terms of geometry, performance, systematic and statistical errors. It is shown that an analysis method previously developed for (S)TEM called conceptEM can also successfully be applied to APFIM data.

1. Introduction

Grain boundary segregation describes the accumulation of foreign atoms at internal boundaries between different grains of polycrystalline material. It is relevant in metallurgy, being responsible for the brittle fracture of structural alloys, and also in electronics, influencing the conductivity of polycrystalline semiconductors in photovoltaic cells and varistor devices.

While qualitative evidence of grain boundary segregation can be readily obtained by breaking the material under ultra-high vacuum conditions to expose these grain boundaries without cross-contamination prior to surface analysis by, e.g. Auger electron spectroscopy [1,2], a quantitative measurement of the interfacial excess of atoms at internal boundaries in the bulk is only possible by two techniques: tomographic atom probe field ion microscopy (APFIM) which combines pulsed field evaporation and time-of-flight mass spectroscopy with a position-sensitive detector, and analytical scanning transmission electron microscopy (STEM). The latter can employ energy-dispersive X-ray spectroscopy (EDX) and/or electron energy-loss spectroscopy (EELS). Both APFIM and STEM can measure grain boundary excess to fractions of monolayer occupation.

This study compares recent developments of both methods, which have extended the capabilities and improved the detection limits, down to ~0.1 atoms/nm^2. For APFIM, the improvements have relied on faster pulse processors and equipment for data acquisition in the MHz range [3], which has increased the total number of atoms analysed in a typical single-run experiment by 2-3 orders of magnitude, from a few 10^3 to a few 10^6. For EDX-STEM the incorporation of multiple X-ray detectors closer to the sample stage has increased the total collection angle and hence the registered count rate

Content from this work may be used under the terms of the Creative Commons Attribution 3.0 licence. Any further distribution of this work must maintain attribution to the author(s) and the title of the work, journal citation and DOI.
Published under licence by IOP Publishing Ltd

by up to a factor of 14 (from 0.12 sr to 0.9 sr [4] or even 1.7 sr [5]), cold field-emission guns offer perhaps 3-4 times higher brightness than conventional Schottky cathodes and as specimen stages have become more stable thermal drift has been reduced so experiments can now be run for extended times. The central question whether a 100-1000 times higher signal will automatically result in a 10-30 times better signal-to-noise (SNR) in both techniques that can directly translate into higher accuracy will be investigated in this study with the help of simulations for APFIM that are analogous to previous simulations for STEM. It will be shown that for both methods

(a) the geometrical constraints for quantitative analysis are actually quite similar [6, 7],
(b) counting more atoms over a larger volume will improve statistical errors but increases systematic errors in both methods,
(c) the ultimate accuracy will no longer be limited by the signal-to-noise ratio as in the past (statistical errors will be reduced) but by uncertainties in the relative detector sensitivity factors which will govern the systematic errors that now typically dominate.

2. Simulations

As can be seen from a comparison of Figures 1 & 2, the geometry for APFIM and STEM-energy-dispersive X-ray spectroscopy (EDXS) data collection and interpretation is similar in that both methods [6,7] consider a cylindrical volume of analysis containing the grain boundary plane (marked hatched) in its centre, however, in APFIM the grain boundary is oriented perpendicular to the long axis, giving an elliptical (and ideally, round) cross-section with the cylinder of analysis while in STEM it is oriented edge-on to the electron beam, parallel to the cylinder's long axis, forming a rectangular cross-section with the cylinder. Consequently, data evaluation typically proceeds in different steps. The simulations for APFIM shown in the following, as well as previous simulations for STEM-EDXS, have been numerically performed in Semper [8] by modelling a cylindrical volume of material consisting of atomic planes populated by individual point-like atoms (Ga, As and Si for GaAs:Si) at the correct density that are then either sampled by successive individual atomic plane removal and atom counting with a certain detector efficiency to simulate APFIM or by successive electron beam propagation, elastic scattering and beam broadening based on a simple multi-slice approach, accompanied by X-ray generation at various depths and detection under a given take-off angle for STEM-EDXS.

2.1 STEM data evaluation by fitting of matrix/solute ratio as function of beam radius

The conceptEM method [9] developed in [10] plots the ratio, R, of matrix (index: m) to solute (index: s) atom counts as function of the radius, r, of the illuminated area. The number of matrix atoms is given by the cylinder volume of radius r and thickness t covered by the matrix (minus the interface plane itself, i.e. $[\pi r^2 - 2rd]t$), multiplied with the corresponding k-factor and the concentration of the matrix atoms, $k_m\,(1-x)$. The number of solute atoms is given by the effective width of the grain boundary or interface, d, multiplied by its area $2rt$, and the k-factor of the solute atoms, k_s, plus the volume fraction covered by the solute concentration x outside the grain boundary. Hence, R is independent of specimen thickness t, and the approximation in equation (1) holds for $x \rightarrow 0$ and $d << r$:

$$R = I_m/I_s = [k_m(1-x)(\pi r^2 - 2rd)]/[k_s(2rd + \pi r^2 x)] \approx [k_m \pi r]/[2k_s d] - k_m/k_s, \qquad (1)$$

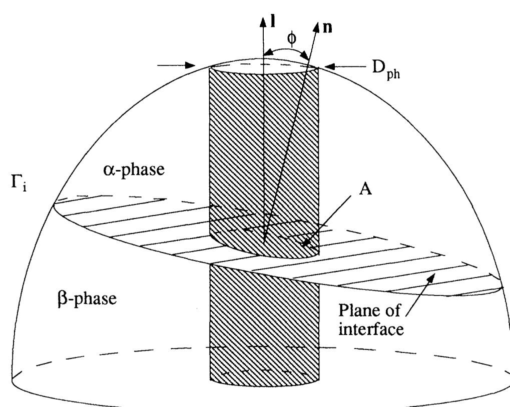

Figure 1. Schematic of APFIM geometry. Reprinted with permission from [6] https://doi.org/10.1103/PhysRevB.48.6724. Copyright (1993) by American Physical Society. α and β denote phases either side of the grain boundary, Γ_i the solute excess at the interface, Φ the inclination of interface normal $\boldsymbol{n}$ with respect to direction $\boldsymbol{l}=-\boldsymbol{z}$ of cylinder axis, D_{ph} the diameter of the cylinder.

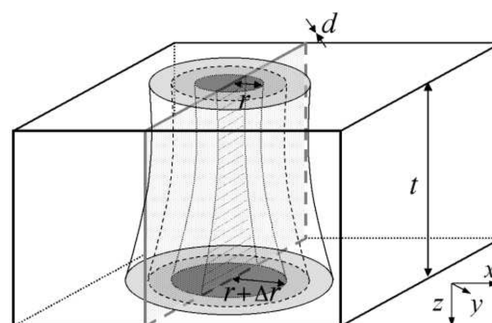

Figure 2. Schematic of STEM-EDXS geometry. Reprinted from [7]. For STEM-EELS it is similar, with less beam broadening towards the exit surface. r is beam radius at the top, Δr is beam broadening at the exit surface, t specimen thickness, z the electron beam direction and (x,y) the habit plane of both surfaces.

Herein the k-factor describes a calibrated sensitivity factor, and only the ratio $k_m/k_s=k_{m,s}$ is relevant. So if one plots the k-factor corrected count ratio $Rk_s/k_m \approx \pi r/(2d)-1$ vs radius r one obtains a linear relationship where the effective width of the grain boundary excess d is given as the inverse of the slope multiplied by a geometric factor $\pi/2$. Beam broadening with thickness introduces a non-linearity in equation (1), which can be used as a direct measure of the systematic error of the method [10]. In [11] it was shown that the method can also be applied to square tetragonal boxes of dimensions $L=2r \times 2r \times t$ instead of cylinders as sketched here, and that the effect of this is that the factor $\pi/2$ in the above equation vanishes so the grain boundary excess d is simply the inverse of the slope of the function $R(L)$. This tetragonal rather than the equivalent cylindrical geometry is used in the following APFIM simulations.

The conceptEM method has been successively applied by the author and colleagues to a number of different systems, including inversion domain boundaries in zinc oxide doped with oxides of antimony [12], tin [13], gallium [14] and iron [15], epitaxial thin films consisting of the semiconductors In(As)P [16], (In)GaAs [17,18], Si(Ge) [19,20] and a $\Sigma=3\{111\}$ Si grain boundary doped with Ga and As [21]. The success of measuring fractions of monolayer occupation by the solute as effective thicknesses, corresponding to typically 0.1-0.8 atom/nm^2 in the above studies, has been made possible due to the insensitivity of the method on how the illuminated area is precisely measured, as long as incremental changes in illumination size can be measured accurately [22], and by the development of a new method to measure self-consistently thickness-corrected relative k-factors based on K/L intensity ratios [23] for Si(Ge) [24], (In)GaAs [25] and (In)GaN [26] to typically 4 % or better, which were previously in error by 12-19 % [27]. The k-factor precision determines the calibration of the vertical axis (R) and the magnification calibration that of the horizontal axis (r or L).

2.2 APFIM data evaluation by fitting ladder diagrams

In APFIM the number of solute atoms (index: s) is plotted vs. total number of atoms along the direction z of the cylinder long axis [6]. This gives a so-called ladder diagram, as shown in Figure 3.

For the test simulation a rectangular box (100×100×200) nm^3 in size has been set up, with 87.5 million atoms in total, describing silicon doped gallium arsenide (GaAs:Si) with a bulk solubility of

silicon of 5×10^{-5}=50 ppm on the group III sub-lattice (i.e. x=2.5×10^{-5} = 25 ppm in total) wherein a single monolayer on a (001) plane with an areal density of 6.25 group III atoms/nm^2 has been covered by ¼ of Si atoms and ¾ of Ga atoms, giving an interfacial excess of Γ_{in} =1.563 Si atoms/nm^2. The slope of the shoulders left and right in the figure gives the modelled solute solubility (=increase of number of Si atoms relative to all atoms), here x=4.9×10^{-5}=49 ppm. The step height yields the number of excess Si atoms at the interface, which must be divided by the cross-sectional area of the interface plane, giving $\Gamma_{\text{out, ideal}}$ =15,635 atoms/(100nm)^2 =1.564 atoms/nm^2.

Clearly, if a smaller volume were analysed, fewer atoms would be counted, and noise would appear that would make the numerical results scatter simply because of counting statistics. This is shown in Figure 4 for three different sub-regions centred about the grain boundary within the simulated box, each with roughly the same number of atoms in total but of different aspect ratios. Box A describes a flat, box B an elongated and box C a box that extends below and above the grain boundary by an amount equal to its height. The numerical results scatter rather widely (A: 1.69 atoms/nm^2, B: 1.00 atoms/nm^2, C: 1.24 atoms/nm^2), in agreement with what has been observed experimentally in the past for silicon [6] and also, more recently, for carbon segregation in steel [28].

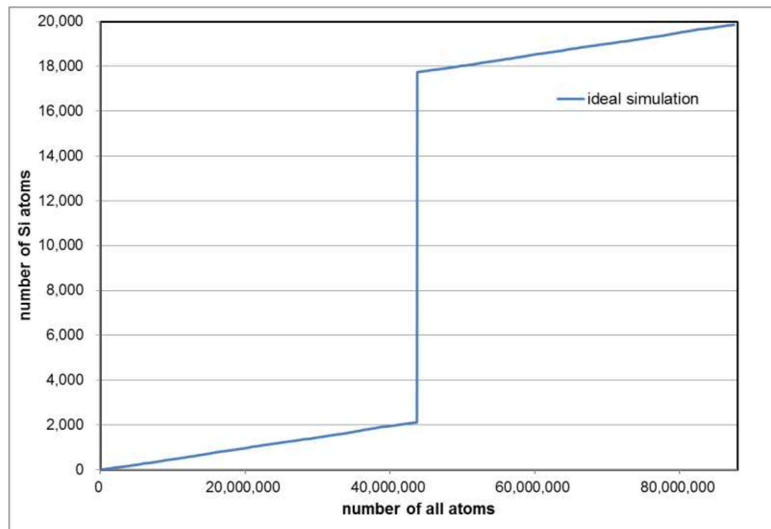

Figure 3. APFIM simulation of GaAs:Si with 87.5×10^6 atoms, $x = 2.5\times10^{-5}$, no interface broadening, distortion-free geometry and ideal detector (η = 1 for all atom types).

The ultimate detection limit expected from Figure 3, defined according to the Rose criterion [29] as a step height 4-5 times the fluctuations of Poisson noise from atom counting statistics above the signal from surrounding bulk (3-4 Si atoms on average), would be ~20 Si atoms per (100 nm)^2, i.e. 0.002 atoms/nm^2. It will be shown that for any realistic APFIM this limit will not be attainable in practice.

This is partly due to finite detection efficiency, η, of the multi-channel detectors in APFIM, which typically lies in the range of 0.5-0.8 [3]. For GaAs, Di Russo et al. [30] showed that $\eta\approx0.6$ but was also depending on the local DC fields and differed for Ga and As atoms by at least 6 %, the precise values being a function of bias and event pile-ups due to correlated evaporation events for neighbouring atoms and ions.

The combined statistical effects of a finite detection probability and finite resolution (in terms of either a real diffusional static displacement or an apparent spread of Si atoms a few atomic planes about the interface plane) may be described by a Gaussian curve of 1nm root-mean-square (rms) in z-direction) and are investigated in Figures 5-8 where, for the same geometry, results are systematically compared for differently sized analysis boxes of the same aspect ratio. As fixed parameters x=2.5×10^{-5}, η=0.60 for Ga and Si, η=0.65 for As atoms have been assumed. While one would expect that an increase of

number of atoms detected by one order of magnitude would simply improve the signal-to-noise ratio by $\sqrt{10}\approx 3$, it can also be observed that the slopes of the linear sections on either side of the interface plane reduce with apparent atom number, indicating that if the number of Si atoms per atomic plane evaporated becomes smaller than a critical value below unity, then relatively more and more of those few Si atoms dissolved in the GaAs matrix or diffused away from the grain boundary plane can no longer be detected at all. This is interpreted as a sampling effect, as only integer number of atoms can be detected, the smallest values being 0 and 1, but no fractional atoms can be counted.

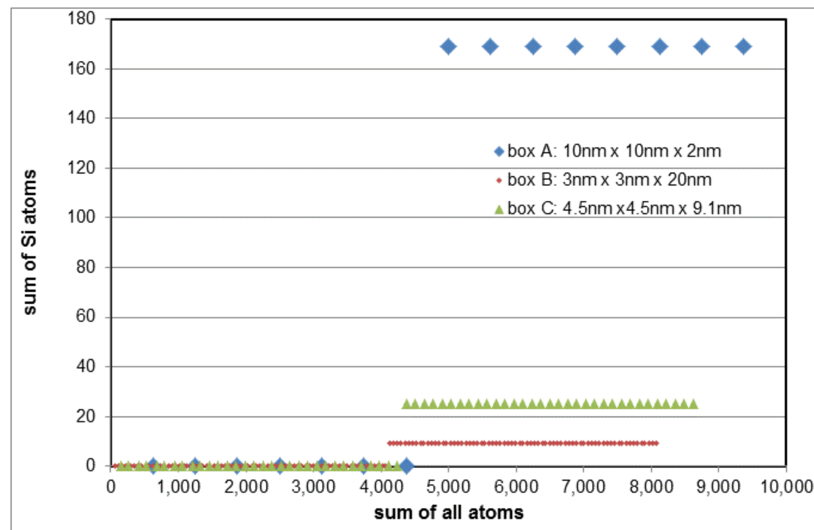

Figure 4. APFIM simulation of GaAs:Si: extraction of boxes of different dimensions $x \times y \times z$ that all contain just under 10,000 atoms in a volume of ~200 nm^3; no interface broadening, distortion-free geometry and ideal detector ($\eta = 1$ for all atom types). The interfacial excess measured is given by the vertical offset divided by the size of the interface contained, i.e. by the product $x \times y$.

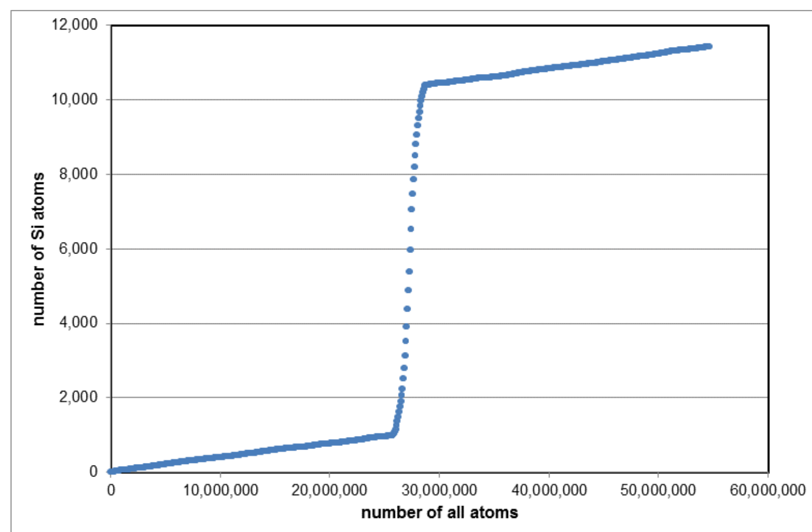

Figure 5. APFIM simulations of GaAs:Si as before with 54,706,600 detected atoms, $x = 2.5\times10^{-5}$, 1 nm interface broadening, distortion-free geometry, $\eta = 0.65$ for As and $\eta = 0.60$ for Ga and Si.

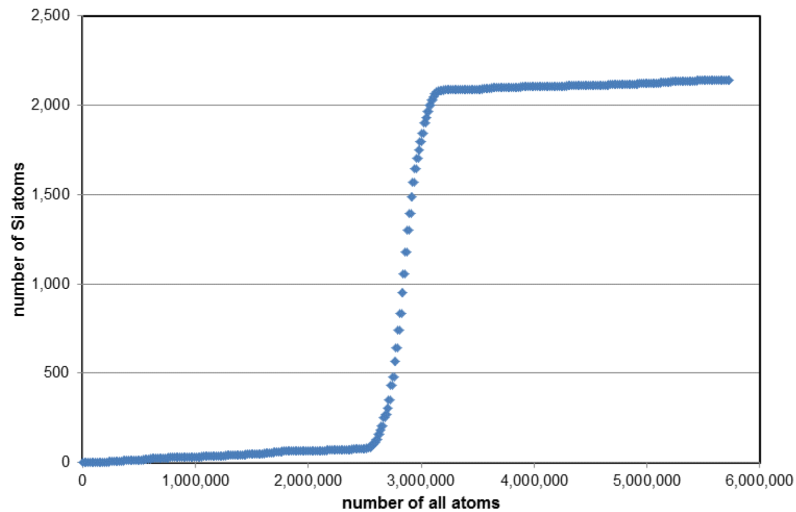

Figure 6. APFIM simulations of GaAs:Si as before with 5,733,430 detected atoms, $x = 2.5\times10^{-5}$, 1 nm interface broadening, distortion-free geometry, $\eta = 0.65$ for As and $\eta = 0.60$ for Ga and Si.

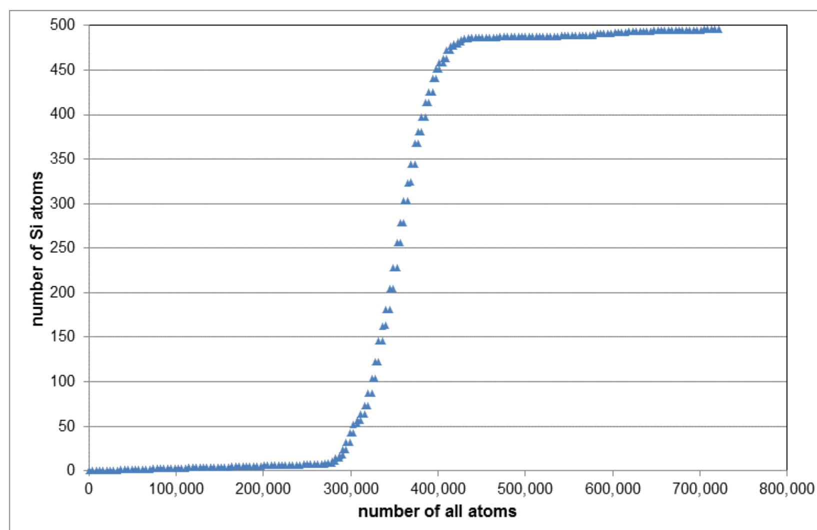

Figure 7. APFIM simulations of GaAs:Si as before with 721,232 detected atoms, $x = 2.5\times10^{-5}$, 1 nm interface broadening, distortion-free geometry, $\eta = 0.65$ for As and $\eta = 0.60$ for Ga and Si.

Converting the offsets into grain boundary excess using the areal values for the corresponding boxes, and dividing the measured results by 0.6 to account for the detection efficiency yields vastly different numerical values, of 1.547 (Figure 5), 1.437 (Figure 6), 1.380 (Figure 7) and 1.308 (Figure 8) Si atoms/nm^2, where only the first value is close to the correct input value of 1.563 Si atoms/nm^2. The scatter of these answers would suggest a grain boundary excess of Γ_{APFIM}=1.42±0.10 Si atoms/nm^2, i.e. an 11 % underestimate due to the counting effect.

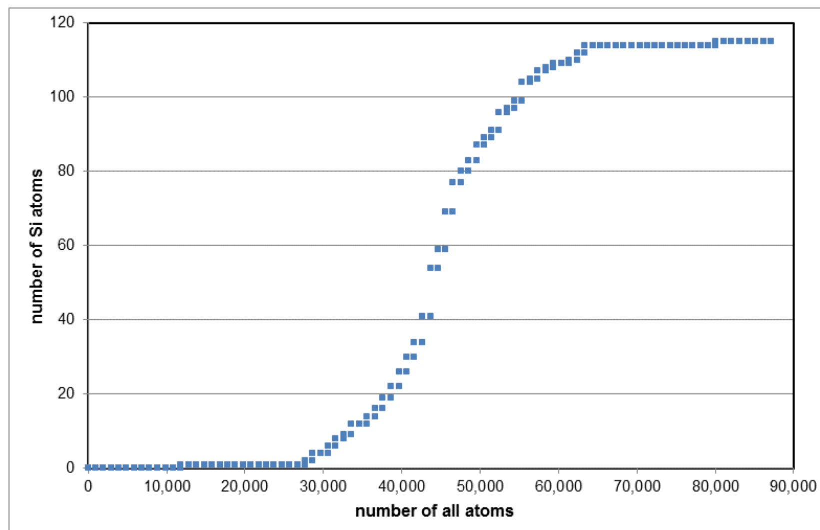

Figure 8. APFIM simulations of GaAs:Si as before with 87,120 detected atoms, x =2.5×10^{-5}, 1 nm interface broadening, distortion-free geometry, η = 0.65 for As and η = 0.60 for Ga and Si.

In Figure 8 one can also discern a clear splitting into two parallel curves. This is due to the fact that the Si atoms are co-located with the Ga atoms on the group III sub-lattice only; so whenever a lattice plane of As atoms is encountered and added to the counts then this increases the total number of atoms counted along the horizontal but not that of Si atoms plotted on the vertical. This is also clear in Figure 9 which plots, for η = 1 and the large box that gave the data in Figure 3 but with the Gaussian static atomic displacements of 1nm rms included, profiles of the number of counted atoms for a small section of 201 atomic planes (corresponding to ~2.8nm) along the z-direction centred about the interface plane of the grain boundary. The data points have been displayed by small squares, and those for Si and Ga are exactly correlated with each other while those for As are displaced by exactly 1 monolayer, corresponding to the relative shift of the group III and group V sub-lattices.

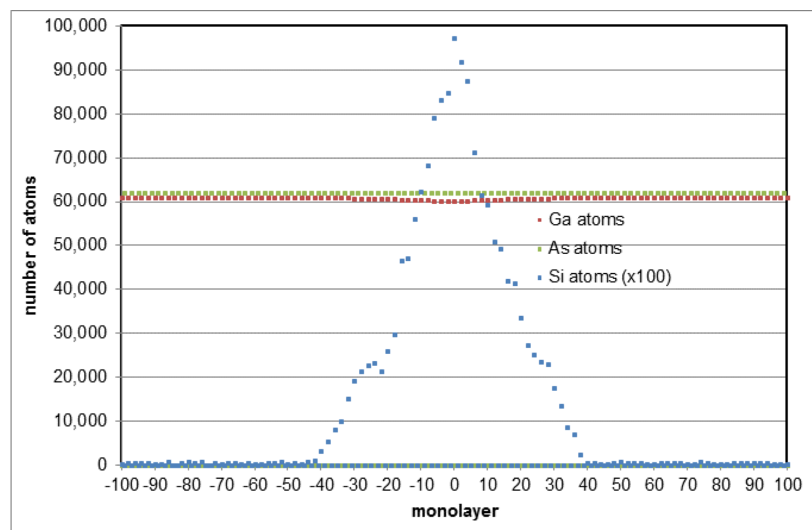

Figure 9. Side view of APFIM simulation with number of atoms per monolayer along z direction (only central 201 of 1414 monolayers in total, i.e. ±100 monolayers around interface, are shown)

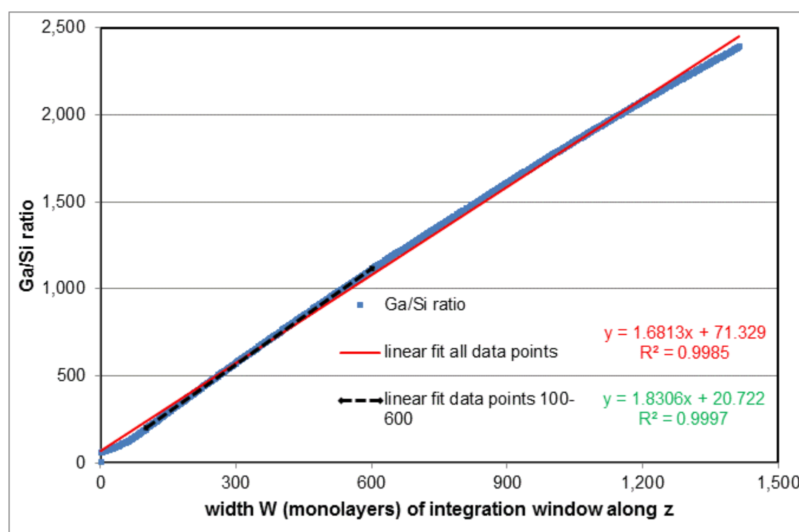

Figure 10. Plot of Ga/Si as function of width *W* of integration window along *z* direction

Figure 10 then plots for this side-on view the ratio of Ga/Si atoms counted in a window extending a total width, *W*, along the *z* direction and centred on the interface plane, which is thus equivalent to what an edge-on STEM analysis would have given wherein different scan windows and probe locations along the interface had been used. Applying now the conceptEM rather than the ladder approach to the APFIM data, we can perform linear fitting to the data over various ranges. Near the origin, the curve bends due to the finite spread of the Si atoms along the *z*-direction modelled. For large integration windows the curvature is in the opposite direction due to the finite solid solubility [10]. Measuring the linearity piece-wise by regression analysis of sections by moving the upper and lower boundaries, one can plot the slope of each fit vs its R^2 fit parameter in Figure 11. The highest R^2 values of 0.9997-0.9998 (green data points) would give a slope of 1.77±0.04, which must be inverted and then divided by a factor 2 (to account for the fact that in Figure 10 the vertical plots the Ga/Si ratio of the group III sub-lattice only while the horizontal contains all monolayers, atoms from groups III and V). This yields 0.283±0.006 ML, or Γ_{STEM}=1.77±0.04 Si atoms/nm^2, which is a 13 % overestimate due to the finite solubility.

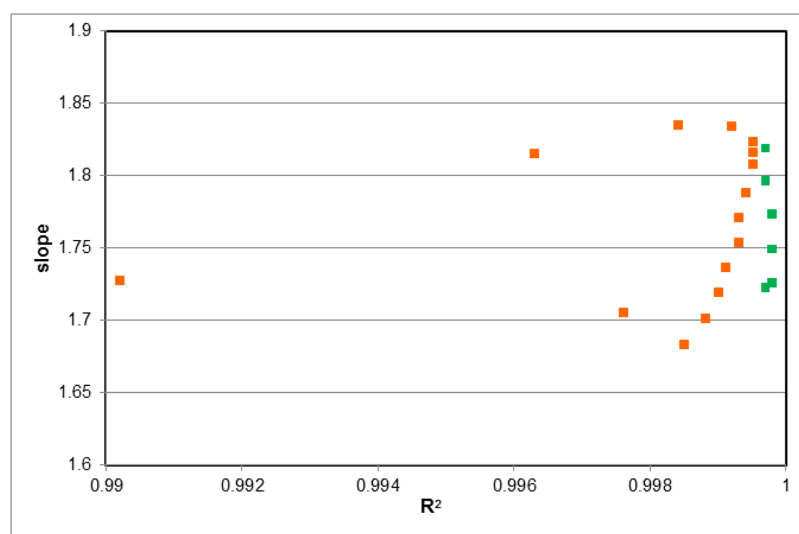

Figure 11. **R**esults from piece-wise linear regression fits Figure 10. Best fits shown in green.

3. Discussion and Conclusion

While it seems intriguing that APFIM counts atoms directly rather than secondary signals, such as X-rays (in STEM-EDXS) or ionisation events (in STEM-EELS), stating that it 'has the advantage that the atoms, field evaporated as ions, are simply identified by their mass-to-charge ratio through time-of-flight spectroscopy, which renders the analysis of absolute concentration values comparably robust' [31] is misleading as it disregards a number of effects that introduce systematic errors also in APFIM:

i. There is no ideal detector, and the detector efficiency η is usually only somewhere between 0.5 and 0.8 [3], meaning many atoms are not registered at all as they either evaporate as neutral atoms or in complexes or as ions that may hit the frame structuring the entrance to the detector pixels. This means the statistics is much worse than anticipated from Figure 3 and typically more similar to that sketched in Figures 6 or 7. Gault et al. [32] carefully measured their average detector efficiency but could nevertheless only conclude that $\eta=0.65\pm0.07$.
ii. The detection sensitivity depends on the ion type and can vary significantly between different species. It also depends on the applied bias, e.g. the apparent Ga/As ratio in pure GaAs can vary from 0.70 to 1.14 and is difficult to control to better than 0.92±0.06 [30]. Pile-ups due to correlated field evaporation of neighbour atoms can reduce the detection of such atoms further.
iii. For GaAs, evaporation of As clusters at high fields varies with surface reconstruction and radius of the field-emitting tip [30], that itself will change during analysis: most tips have a non-zero shank angle so their radius increases gradually during evaporation, in turn reducing field strength [32].
iv. As the tip radius evolves, the effective magnification of the point projection image changes. While APFIM can reach lattice resolution in the z-direction perpendicular to the detector plane, resolution in the detector (x,y)-plane is much worse, often only a few nm, and can change easily without being noticed. For a tip radius change of 6 % relative, as in [32], the lateral magnification will change by 6 % in x and in y, so the area of the cross-section that contains the interface of interest will change by a massive 12 %. The precision with which the lateral magnification can be calibrated in APFIM is probably much worse than for STEM where lattice planes are readily imaged, and it enters the APFIM ladder approach in square while it enters the conceptEM ratio approach only linearly.

In summary, if one assumes only a 3 % variability of the detection efficiency with atomic species, and a change in tip radius of also 3 %, then this alone will give a systematic relative error of ~10 %, which in practice could be twice as high for GaAs, as outlined above. The key message is that if one wants to improve the statistics, then the only way to do this is to enlarge the measured volume, which however means the systematic errors due to tip blunting etc will increase. This explains why the relative errors in many experiments remained 20-30 % even for $\sim2\times10^6$ atoms analysed in [33]; so the absolute errors for strongly segregated species remained large while the detection limit for hardly segregated species can became small. The only notable exception in [33] was boron detection at general grain boundaries in steel, for which an incredibly precise value of $\Gamma= 0.53\pm0.01$ B atoms/nm^2 was reported, albeit without any evidence. APFIM simulations suggest the ladder approach underestimates the segregated interface excess by an amount that depends on the actual analysis volume.

The conceptEM ratio plot analysis previously developed for (S)TEM seems to give a corresponding overestimate when applied to APFIM data, with the advantage of an inherent error estimate via the R^2 parameters.

The experimental limitations of (S)TEM on the other hand are mainly given by beam broadening and finite solubility limits as shown in [10], to which further experimental problems like specimen contamination [34] and drift during acquisition as well as radiation sensitivity of the material studied can add.

Hence, none of the two methods is generally superior to the other; the main point of this study is to highlight that, at least for Si segregation in GaAs, APFIM data can be better quantified using the conceptEM approach originally developed for (S)TEM instead of the more traditional ladder approach.

References

[1] Harris LA 1968 *J. Appl. Phys.* **39**, 1428-1431.
[2] Seah MP and Hondros ED 1973 *Proc. Roy. Soc. Lond. A* **335**, 191-212.
[3] CAMECA LEAP 5000 broschure 2015, information on efficiencies of LEAP 5000 XR (η=0.5) and XS (η =0.8), available online at https://www.cameca.com/products/apt/leap5000
[4] FEI application note 11006-4390 for Tecnai Osiris 2010 *ChemiSTEM technology: a revolution in EDX analytics*, also online at https://www.fei.com/documents/talos-f200x-datasheet/
[5] Yamazaki K 2016 *JEOL News* **51**, 49; also JEOL specification EM-1526B for JEM-F200 HR with dual 100 mm^2 SDD
[6] Krakauer BW and Seidman DN 1993 *Phys. Rev. B* **48**, 6724-6727.
[7] Walther T, Daneu N and Recnik A 2004 *Interface Sci.* **12**, 267-275.
[8] Saxton WO, Pitt TJ and Horner M 1979 *Ultramcroscopy* **4**, 343-353.
[9] Walther T, Recnik A, Daneu N 2005 Proc. MSM-14, Oxford. *Springer Procs. Phys.* **107**, 199-202.
[10] Walther T 2004 *J. Microsc.* **215**, 191-202.
[11] Walther T 2006 *J. Microsc.* **223**, 165-170.
[12] Recnik A, Daneu N, Walther T and Mader W 2001 *J. Am. Ceram. Soc.* **84**, 2657-2668.
[13] Daneu N, Recnik A, Walther T and Mader W 2003 Proc. MC2003, Dresden. *Microsc. Microanal.* **9** S 3, 286-287.
[14] Barf J, Walther T and Mader W 2004 *Interface Sci.* **12**, 213-226.
[15] Walther T, Wolf F, Mader W and Recnik A 2006 *Int. J. Mater. Res.* **97**, 934-942.
[16] Walther T 2007 Proc. MSM-15, Cambridge. *Springer Procs. Phys.* **120**, 247-250
[17] Walther T 2008 Proc. EMAG2007, Glasgow. *J. Phys.: Conf. Ser.* **126**, 012091.
[18] Walther T 2015 *phys. stat. sol. (c)* **12**, 310-313.
[19] Norris DJ, Qiu Y, Dobbie A, Myronov M and Walther T 2014 *J. Appl. Phys.* **115**, 012003.
[20] Norris DJ and Walther T 2018 *Mater. Sci. Technol.* **34**, 1539-1548.
[21] Walther T, Hopkinson M, Daneu N, Recnik A, Ohno Y, Inoue K and Yonenaga I 2014 *J. Mater. Sci.* **49**, 3898-3908.
[22] Walther T, Recnik A and Daneu N 2006 *Microchim. Acta* **155**, 313-318.
[23] Walther T and Wang X 2015 Proc. EMAG 2015, Manchester. *J. Phys. Conf. Ser.* **644**, 012006.
[24] Qiu Y, Nguyen VH, Dobbie A, Myronov M and Walther T 2013 Proc. MSM-18, Oxford. *J. Phys. Conf. Ser.* **471**, 012031.
[25] Parri MC, Qiu Y and Walther T 2015 *J. Microsc.* **260**, 427-441.
[26] Walther T and Wang X 2016 *J. Microsc*. **262**, 151-156.
[27] Walther T 2010 Proc. MSM-16, Oxford. *J. Phys. Conf. Ser.* **209**, 012029.
[28] Herbig M, Raabe D, Li YJ, Choi P, Zaefferer and Goto S 2014 *Phys. Rev. Lett.* **112**, 126103.
[29] Rose A 1948 *J. Opt. Soc. Am.* **38**, 196-208.
[30] Di Russo E, Blum I, Houard J, Da Costa G, Blavette D and Rigutti L 2017 *Microsc. Microanal.* **23**, 1067-1075.
[31] Herbig M, Choi P and Raabe D 2015 *Ultramicroscopy* **153**, 32-39.
[32] Gault B, de Geuser F, Stephenson LT, Moody MP, Buddle BC and Ringer SP 2008 *Microsc. Microanal.* **14**, 296-305.
[33] Herbig M, Kuzmina M, Haase C, Marceau RKW et al. 2015 *Acta mater.* **83**, 37-47.
[34] Griffiths AJV and Walther T 2010 Proc. EMAG2009, Sheffield. *J. Phys. Conf. Ser.* **241**, 012017.